BIOSYNTHESIZED SILVER NANOPARTICLES FROM *ABRUS PRECATORIUS*: SUBACUTE TOXICITY ASSESSMENT AND BIOIMAGING ANALYSIS FOR ENHANCED PHARMACOLOGICAL INSIGHT

Supported by tetfund TERTIARY EDUCATION TRUST FUND

Stephenie. C. Alaribe[1*], Blessing E. Titilayo[1], Felicia N. Ejiah[2], Victor. A. Oloruntoba, Sunday O. Okoh[3], Daniel D. Osiagwu[4], Mike O. Ojemaye[5], O. B. Familoni[2] and Anthony I. Okoh[6]

[1]Department of Pharmaceutical Chemistry, Faculty of Pharmacy, College of Medicine Campus, University of Lagos.

[2]Department of Chemistry, University of Lagos, Akoka, Lagos, Nigeria

[3]CFET Department, Federal Institute of Industrial Research Oshodi, Lagos, Nigeria

[4]Department of Anatomic and Molecular Pathology, College of Medicine Campus, Idi-Araba LUTH, University of Lagos

[5]Department of Pure and Applied Chemistry, University of Fort Hare, Alice, South Africa

[6]Applied and Environmental Microbiology Group (AEMREG), Department of Biochemistry and Microbiology, University of Fort Hare, Private Mail Bag X1314, Alice 5700, South Africa

Corresponding author's e-mail: salaribe@unilag.edu.ng

Received: May 09, 2024 Accepted: June 25, 2024

Abstract: This research investigates the safety of biosynthesized silver nanoparticles derived from *Abrus precatorius* seeds and husk. Characterization of the nanoparticles and crude extracts was conducted using UV-visible absorption spectrophotometry, Fourier transform infrared spectrophotometry, transmission electron microscopy, scanning electron microscopy, and X-ray diffractometry. Subacute toxicity was assessed by administering doses of 0.07 mg/kg, 0.20 mg/kg, and 0.60 mg/kg to the test animals, with normal saline as the control. Hematological and histopathological analysis was carried out on the blood samples and selected organs. Results indicated that the nanoparticles were significantly less toxic than crude extracts, with the lowest dose (0.07 mg/kg) of the biosynthesized nanoparticle from the husk showing minimal effects on glomerular and Bowman's capsule regions compared to controls. Additionally, a dose lower than 0.07 mg/kg of the biosynthesized silver nanoparticles and crude samples of *A. precatorius* is expected to be a much safer choice in repeated-dose studies assessing the numerous therapeutic effects of intraperitoneal administration. This study suggests that biosynthesized silver nanoparticles from *Abrus precatorius* are a safer alternative to its crude extracts for pharmacological applications and warrant further clinical investigation.

Keywords: *Abrus precatorius*, biosynthesized, silver nanoparticle, nanotoxicity, bioimaging analysis

Introduction

Due to the recent quick evolution of various diseases through mutation and the rapid emergence of drug resistance to antibiotics, anti-cancer, anti-malarial drugs to mention but a few, hence, the need to search for alternative drugs or methods for controlling resistant pathogens is critical. Advanced research in nanotechnology has recently led to the development of nano-scale drugs with prominent actions against multidrug-resistant pathogens. As a result, the effect must be tested before use. A drug with the best therapeutic activities against a particular infection or disease condition in the laboratory in vitro and in vivo is expected to be safe enough to use at its effective dose. Metal nanoparticles are used in some of the most cutting-edge nano-technological applications because of their particular mechanism of action, which yields the most successful outcomes (Das *et al*. 2020). Silver nanoparticles are increasingly used in various fields, including medical, food, health care, consumer, and industrial purposes, due to their unique physical and chemical properties. (Wong *et al*. 2019). Nanosized metallic particles are unique and can considerably change physical, chemical, and biological properties due to their surface-to-volume ratio; therefore, these nanoparticles have been exploited for various purposes (Cheng *et al*. 2020). In addition to increasing the bioavailability of therapeutic agents after systemic and local administration in nanoparticle form, nanoparticles' physicochemical characteristics can also impact cellular uptake, biological distribution, penetration through biological barriers, and the subsequent therapeutic effects.

In comparison with traditional pathology, digital imaging, and computational analysis offer improved efficiency and robustness in the assessment of toxicity in cells and tissues (Baxi *et al*. 2022; Turner *et al*. 2020). The availability of robust digital image analysis software could reduce time and costs and at the same time increase accuracy and reproducibility (Madabhushi and Lee 2016). The kidneys are the most important organs in the urinary system and some of the most essential in the body for the maintenance of homeostasis and they are responsible for the elimination of toxic substances and wastes from the blood (Emon *et al*. 2021; Tang *et al*. 2020; Clark *et al*. 2019). The basic structural and functional unit of the kidney is called the *nephron* – this contains a primary filter which is called *glomerulus* (Chambers *et al*. 2020; Solomon and Goldstein 2017). The glomerulus is the capillary network formed into a ball-like structure, it is found in the space within the Bowman's capsule called the Bowman's space or urinary space (Arif and Nihalani. 2013). Changes in the size and structure of the Bowman's capsule, Bowman's space, and glomerulus could indicate significant loss of renal function and nephrotoxicity (Yoshiara *et al*. 1993; Chantler and Holliday 1987; Tsuboi *et al*. 2017).

Metal nanoparticles (NPs) are used in some of the most cutting-edge nano-technological applications because of their particular mechanism of action, which yields the most successful outcomes (Rao and Gan 2015). Silver nanoparticles are increasingly used in various fields, including medical, food, health care, consumer, and industrial sectors due to their unique physical and chemical properties (Jorge De Souza *et al*. 2019). Nano-sized metallic particles are unique and can considerably change physical, chemical, and biological properties due to their surface-to-volume ratio; therefore, these nanoparticles have been

exploited for various purposes (Chen and Liang 2020). In addition to increasing the bioavailability of therapeutic agents after systemic and local administration in nanoparticle form, nanoparticles' physicochemical characteristics can also impact cellular uptake, biological distribution, penetration through biological barriers, and the subsequent therapeutic effects.

Despite numerous reports on the biosynthesis of nanoparticles as an eco-friendly and less expensive method of nanoparticle synthesis, as well as their improved therapeutic effects over natural products used, studies on the repeated dose toxicity of biosynthesized nanoparticles are scarce. It is critical to evaluate the safety doses of these biosynthesized nanoparticles, which are potential drug leads, in order to obtain a dose that can be safely used in the evaluation of its therapeutic effects. Furthermore, in addition to traditional histopathology, computational image analysis provides a more accurate, robust, and reproducible result of tissue sections in assessing xenobiotic toxicity.

Methods

Nanoparticle synthesis

Silver nanoparticles were synthesized using the method described by Larayetan *et al*. 2019. Briefly, 1 part of the aqueous extract of the plant part was added to 9 parts of a 0.10 M solution of silver nitrate. The mixture was then left to stir on a magnetic hot plate stirrer at room temperature until a visible colour change and precipitate were noticed. The precipitate was thereafter centrifuged and washed in deionized water to attain a clean nanomaterial. The product was then dried in an oven for 24 h at 105 °C. The biosynthesized nanoparticles were kept in a sealed sample amber bottle awaiting characterization and bioactive assays.

Characterization of the synthesized nanoparticles

The synthesized nanoparticle samples as well as the plant extract absorption spectra were examined with a Perkin-Elmer UV-visible absorption spectrophotometer. A Perkin-Elmer ATR 100 FTIR spectrophotometer was used to obtain the vibrational frequencies of the NP samples and the crude plant extract. The samples' TEM (Transmission electron micrograph) were produced at 100 kV (acceleration voltage) by the JOEL 1210 transmission electron microscope, while we obtained the electron micrograph via the JSM-6390 LVSEM scanning electron microscope (SEM) for the synthesized samples and seed aqueous extract. We also used SEM to amass the EDS (electron diffraction images) of the samples. The Bruker D8 X-ray diffractometer was utilized to confirm and measure the size, phase, and crystallinity of the nanomaterials.

Dose validation

A single dose (0.71 mg/kg) of each sample, labeled as pre-treatment (PT) groups – PTA1, PTA2, PTAB1, and PTB2 was administered to different animals, based on the result of a previous study according to Sunday *et al*, 2013. The mice were observed for signs of toxicity and the observed mortality was recorded. The surviving animals were observed till the end of the study and euthanised

Subacute toxicity study

Four treatment samples and a control were utilized in the study. The treatment samples included two nanoparticles A1 and B1 synthesized via the bio reduction of natural products A2 (shell) and B2 (seed) respectively as well as the natural products A2 and B2 which were administered at three different doses daily (lowest dose-0.07 mg/kg, mid-dose – 0.20 mg/kg, and highest dose – 0.60 mg/kg) through intraperitoneal injection for 28 days. The negative control group received 0.9% normal saline. The mice were monitored for clinical signs of toxicity such as weight loss, dullness, spasms, diarrhea, and grooming over the course of the study. Animals that died during the course of the study had their organs harvested for histopathological examination. During the study, a peripheral blood smear was taken after two days of administration. At the end of the study, the surviving animals were sacrificed and their blood was collected for hematological study, peripheral blood smear was made and bone marrows were collected for micronucleus assay to determine the genotoxicity of the different treatment samples and at different doses.

Organs of the sacrificed animals were also collected for histopathological examination to assess the target organ-directed toxicity of the treatment samples.

Statistics: Computational image analysis was performed on the kidney photomicrographs of all surviving animals using QuPath bioimage analysis software to assess the effect of the treatment samples on the morphology of the Bowman's capsule, Bowman's space, and glomerulus.

Results

Nanoparticle characterization

Upon the completion of the synthesis, different analytical techniques were employed to characterize the products, establish the formation of the nanomaterials, and bioactive potential of the aqueous *A. precatorius*-extracts mediated silver nanoparticles.

Ultraviolet-visible spectroscopy

The addition of plant part extract to silver nitrate to obtain AgNP produces a black colour formation, hence the need for Ultraviolet-Visible spectroscopy measurement (Figure 1A). The UV-Vis study was carried out in distilled water at a concentration of 10^{-3} at room temperature. The compounds were sparingly soluble in water, but on agitation, solubility was achieved.

Fourier transform infrared (FTIR) spectroscopy

The FTIR results are as presented in Figures 1B, 1C, and 1D. The relevant bands' data are depicted in the spectra below (Figures 1B, 1C, and 1D). The FTIR spectra show some characteristic bands assignable to some functional groups observed in the fingerprint and infrared region. The relevant bands' data are depicted in the spectra in Figures 1B, 1C, and 1D.

Scanning electron microscopy, transmission electron microscopy, and energy dispersive X-ray spectroscopy

The Scanning electron microscopy (SEM) and energy dispersive X-ray spectroscopy (EDX) of the seed and shell extracts mediated silver nanoparticles were carried out to reveal the external morphology (Figure 1E and 1F), as well as the biosynthesized nano elemental composition (Figure 5I). The EDX image indicated that silver nanoparticles were synthesized from the plant extract reduction of the silver nitrate salt and the average nanoparticles dimensions are as displayed in Figure 1G and 1H (TEM image).

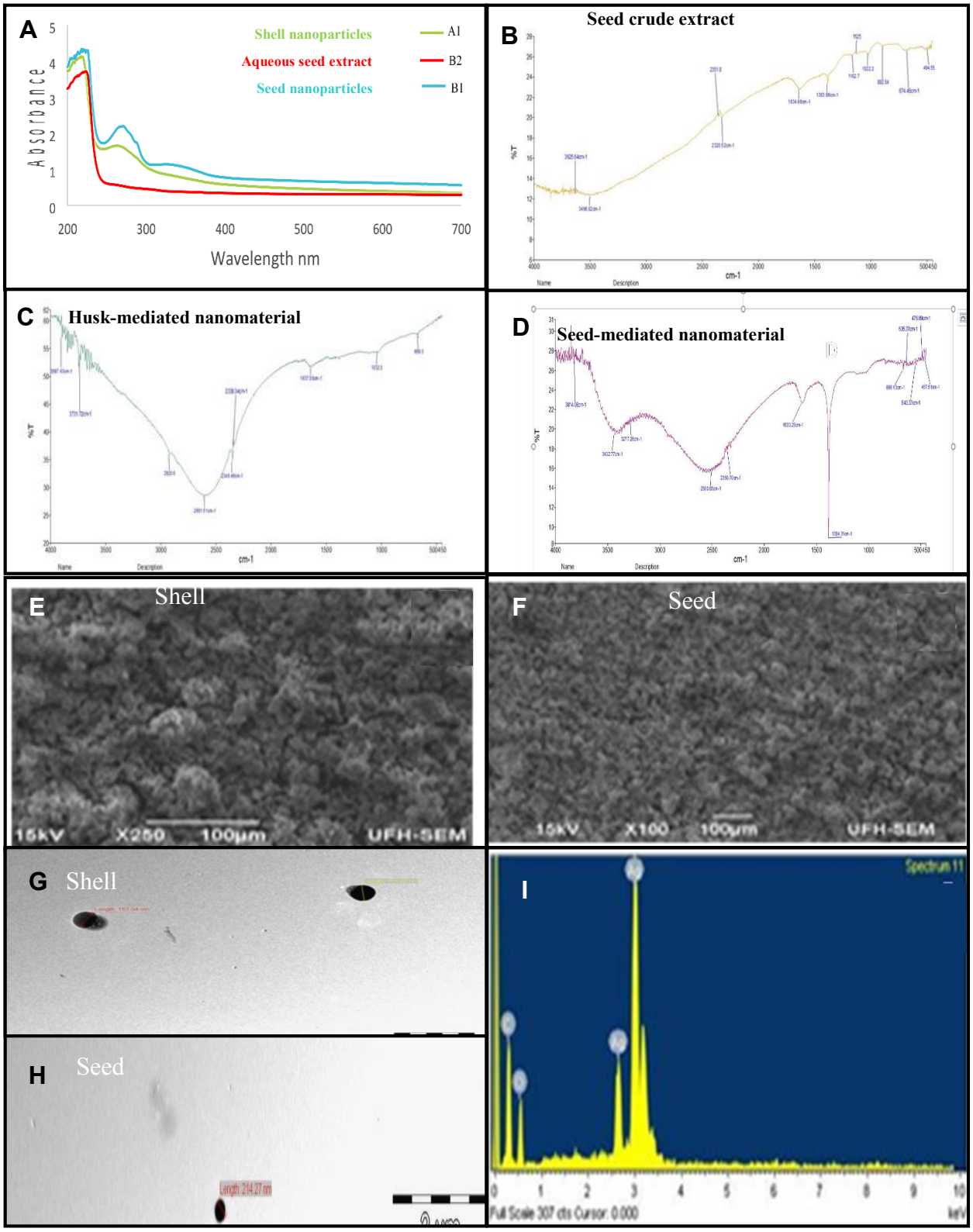

Figure 1: Characterization of *Abrus precatorius* using UV (A), FTIR (B, C and D), SEM (E and F), TEM (G and H), and EDX (I).

HAEMATOLOGICAL ANALYSIS

Table 1 presents the results of the hematological analysis conducted on the mice given sample A1 at different doses.

Table 1: Summary of haematological values of mice given sample A1 and negative control (NC) for 28 days.

Parameters	A1 - 0.07mg/kg	A1 - 0.20mg/kg	A1 - 0.60mg/kg	NC	Normal range
WBC (× 10^3/µL)	6.40 ± 2.00	3.80 ± 1.00	4.80 ± 0.00	4.30 ± 0.00	2-10
Lymph# (× 10^3/µL)	1.35 ± 0.00	1.35 ± 1.00	1.10 ± 1.00	1.20 ± 0.00	2.88-11.15[b]
Mid# (× 10^3/µL)	3.30 ± 1.00	1.10 ± 1.00	1.40 ± 1.00	1.95 ± 0.00	0.43-3.64 [b]
Gran# (× 10^3/µL)	1.75 ± 0.00	1.35 ± 0.00	2.30 ± 1.00	1.15 ± 0.00	0.00-2.66 [b]
Lymph%	20.45 ± 0.00	33.15 ± 6.00	22.70 ± 12.00	28.05 ± 9.00	
Mid%	51.55 ± 1.00	24.95 ± 16.00	29.80 ± 22.00	45.15 ± 6.00	
Gran%	28.00 ± 0.00	41.90 ± 22.00	47.50 ± 10.00	26.80 ± 3.00	
HGB (g/dL)	13.90 ± 0.00	11.65 ± 2.00	10.60 ± 3.00	15.10 ± 0.00	10-17
RBC (× 10^6/µL)	9.49 ± 0.00	6.66 ± 3.00	6.24 ± 3.00	9.75 ± 0.00	7-11
HCT (%)	47.20 ± 1.00	38.25 ± 9.00	35.10 ± 13.00	55.10 ± 3.00	35-52
MCV (fL)	49.75 ± 0.00	63.80 ± 14.00	64.30 ± 15.00	56.55 ± 1.00	45-55
MCH (pg)	14.60 ± 0.00	20.00 ± 6.00	20.00 ± 6.00	15.45 ± 0.00	15-18
MCHC(g/dL)	29.45 ± 1.00	30.95 ± 2.00	30.80 ± 2.00	27.40 ± 1.00	30-38
RDW-CV (%)	18.00 ± 1.00	16.75 ± 1.00	16.05 ± 1.00	19.00 ± 0.00	16-23
RDW-SD (fL)	28.00 ± 0.00	38.85 ± 11.00	35.25 ± 8.00	35.05 ± 1.00	
PLT (× 10^3/µL)	650.00 ± 13.00	339.50 ± 317.00**	414.00 ± 199.00	793.50 ± 53.00	900-1600
MPV (fL)	6.20 ± 0.00	9.20 ± 3.00	7.30 ± 1.00	6.60 ± 1.00	4-6
RDW (%)	14.80 ± 0.00	16.50 ± 2.00	15.30 ± 0.00	16.30 ± 1.00	11-14 or 16-23[a]
PCT (%)	0.41 ± 0.00	0.21 ± 0.00*	0.28 ± 0.00	0.53 ± 0.00	0.36-0.96

*: Significant differences from negative control group * ($p<.05$), ** ($p<.01$), and *** ($p<.001$) WBC: White Blood Cells; Lymph: Lymphocytes; Mid: Other types of white blood cells; Gran: Granulocytes; HGB: Haemoglobin; RBC: Red Blood Cells; HCT: Haematocrit; MCV: Mean Cell Volume; MCH: Mean Cell Haemoglobin; MCHC: Mean Cell Haemoglobin Concentration; RDW: Red cell Distribution Width; PLT: Platelet count; MPV: Mean Platelet Volume; PCT: Plateletcrit; NC: Negative Control. Normal ranges were obtained from The Mouse in Biomedical Research, Volume 3, Second Edition (Ihedioha, 2012; E. Everds, 2007)

Figure 2 presents the results of the hematological analysis conducted on mice administered different doses of samples A1 and A2.

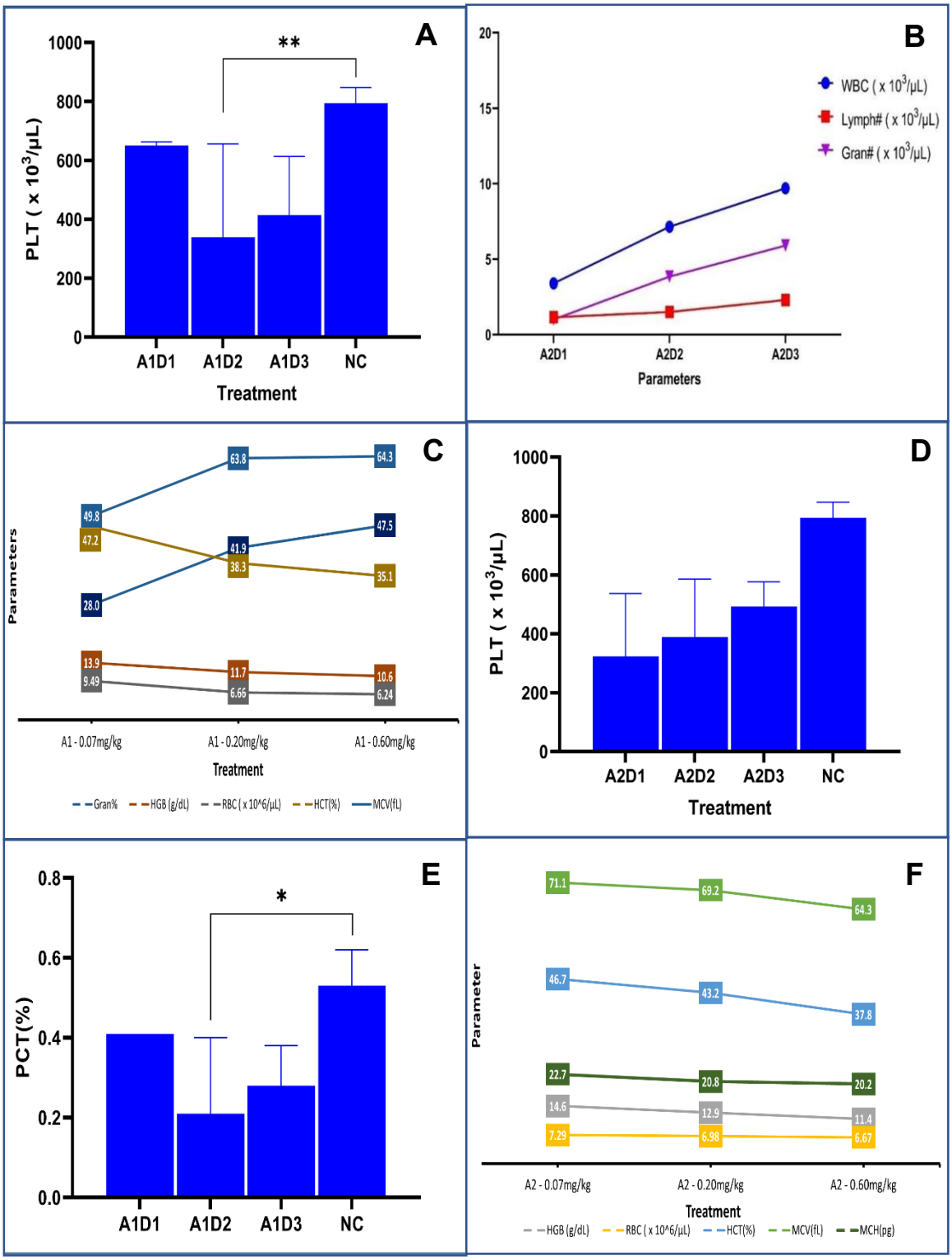

Figure 2: Comparative Impact of A1 and A2 Treatments on Blood Parameters: Platelet Counts (PLT) (A and D), Red Blood Cell Parameters (C and F), and Plateletcrit (PCT) (E).

Table 2 and Figure 3 present the results of the hematological analysis conducted on mice administered different doses of sample.

Table 2: Summary of haematological values of mice given sample A2 and negative control (NC) for 28 days.

Parameters	A2 - 0.07mg/kg	A2 - 0.20mg/kg	A2 - 0.60mg/kg	NC	Normal range
WBC (× 10^3/µL)	3.40 ± 1.00	7.15 ± 3.00	9.70 ± 6.00	4.20 ± 0.00	2-10
Lymph# (× 10^3/µL)	1.15 ± 0.00	1.50 ± 1.00	2.30 ± 1.00	1.50 ± 0.00	2.88-11.15[b]
Mid# (× 10^3/µL)	1.25 ± 1.00	1.80 ± 0.00	1.50 ± 0.00	1.70 ± 0.00	0.43-3.64 [b]
Gran# (× 10^3/µL)	1.00 ± 0.00	3.85 ± 2.00	5.90 ± 5.00	1.00 ± 0.00	0.00-2.66 [b]
Lymph%	39.55 ± 19.00	17.25 ± 11.00	29.75 ± 9.00	36.80 ± 0.00	
Mid%	30.50 ± 20.00	30.70 ± 16.00	26.10 ± 17.00	39.40 ± 0.00	
Gran%	29.95 ± 2.00	52.05 ± 5.00	44.15 ± 27.00	23.80 ± 0.00	
HGB (g/dL)	14.60 ± 1.00	12.90 ± 1.00	11.35 ± 2.00	14.80 ± 0.00	10-17
RBC (× 10^6/µL)	7.29 ± 2.00	6.98 ± 3.00	6.67 ± 3.00	9.51 ± 0.00	7-11
HCT (%)	46.70 ± 1.00	43.20 ± 4.00	37.75 ± 10.00	52.40 ± 0.00	35-52
MCV (fL)	71.05 ± 21.00	69.15 ± 20.00	64.30 ± 16.00	55.10 ± 0.00	45-55
MCH (pg)	22.65 ± 8.00	20.80 ± 6.00	20.15 ± 7.00	15.50 ± 0.00	15-18
MCHC(g/dL)	32.25 ± 3.00	29.85 ± 1.00	30.75 ± 3.00	28.20 ± 0.00	30-38
RDW-CV (%)	15.00 ± 3.00	17.25 ± 0.00	18.75 ± 0.00	19.00 ± 0.00	16-23
RDW-SD (fL)	36.40 ± 8.00	39.65 ± 12.00	40.90 ± 13.00	35.70 ± 0.00	
PLT (× 10^3/µL)	323.50 ± 214.00	389.00 ± 197.00	492.50 ± 85.00	740.00 ± 0.00	900-1600
MPV (fL)	7.65 ± 2.00	7.80 ± 2.00	6.70 ± 1.00	5.90 ± 0.00	4-6
RDW (%)	15.00 ± 1.00	15.05 ± 0.00	15.25 ± 1.00	15.10 ± 0.00	11-14 or 16-23[a]
PCT (%)	0.22 ± 0.00	0.24 ± 0.00	0.32 ± 0.00	0.44 ± 0.00	0.36-0.96

*: Significant differences from negative control group * ($p<.05$), ** ($p<.01$), and *** ($p<.001$) WBC: White Blood Cells; Lymph: Lymphocytes; Mid: Other types of white blood cells; Gran: Granulocytes; HGB: Haemoglobin; RBC: Red Blood Cells; HCT: Haematocrit; MCV: Mean Cell Volume; MCH: Mean Cell Haemoglobin; MCHC: Mean Cell Haemoglobin Concentration; RDW: Red cell Distribution Width; PLT: Platelet count; MPV: Mean Platelet Volume; PCT: Plateletcrit; NC: Negative Control. Normal ranges were obtained from The Mouse in Biomedical Research, Volume 3, Second Edition (Ihedioha, 2012; E. Everds, 2007).

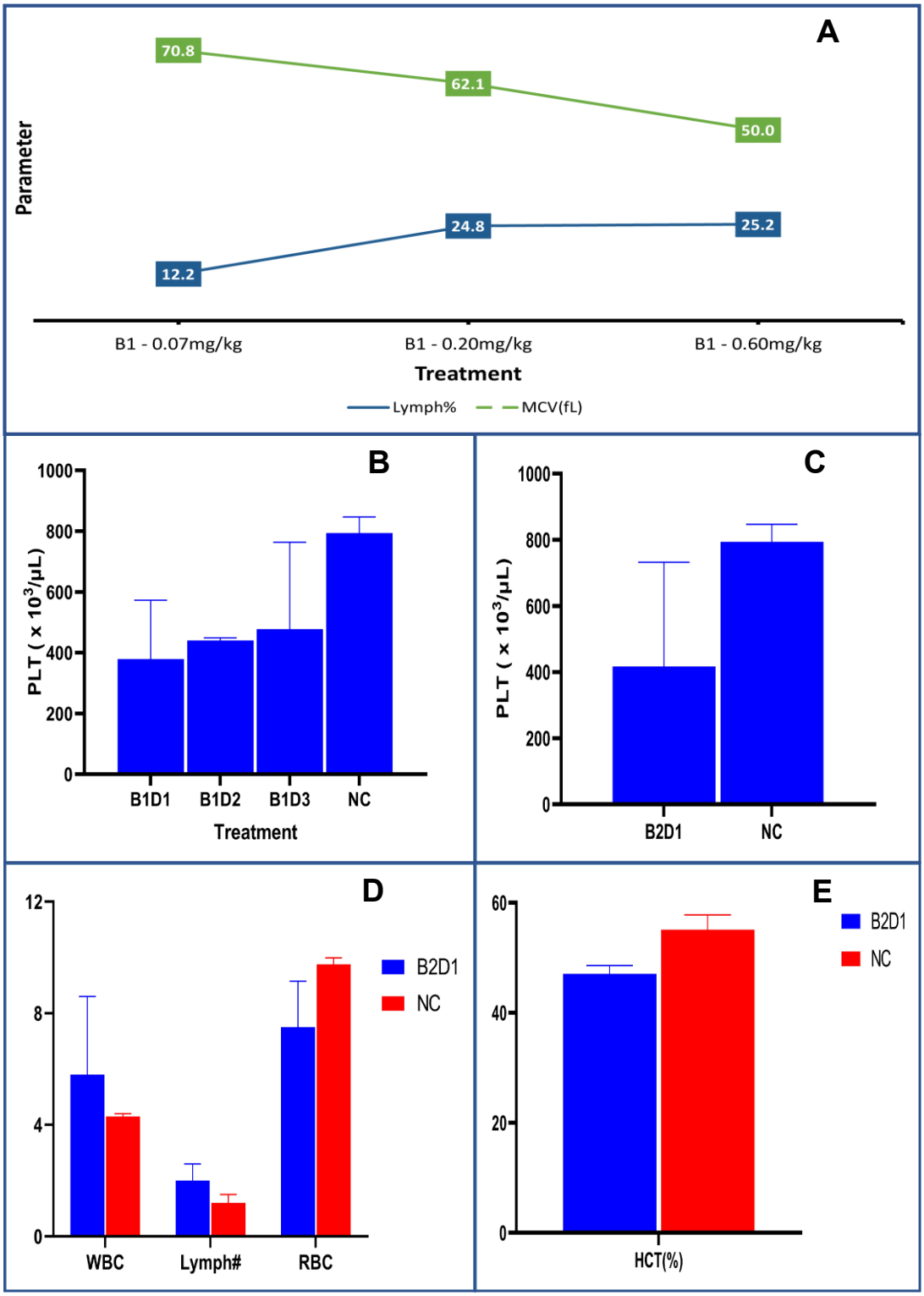

Figure 3: Comparative Impact of B1 and B2 Treatments on Blood Parameters: Platelet Counts (PLT) (B and C), White Blood Cell Parameters A and D, and Hematocrit (HCT) (E).

Table 3 presents the results of the hematological analysis conducted on mice administered different doses of sample B1 and the negative control.

Table 3: Summary of haematological values of mice given sample B1 and negative control (NC) for 28 days.

Parameters	B1 - 0.07mg/kg	B1 - 0.20mg/kg	B1 - 0.60mg/kg	NC	Normal range
WBC (× 10^3/µL)	7.25 ± 1.00	11.70 ± 3.00	6.90 ± 2.00	4.20 ± 0.00	2-10
Lymph# (× 10^3/µL)	0.85 ± 0.00	3.45 ± 3.00	1.65 ± 0.00	1.50 ± 0.00	2.88-11.15[b]
Mid# (× 10^3/µL)	2.45 ± 2.00	2.85 ± 2.00	2.40 ± 2.00	1.70 ± 0.00	0.43-3.64 [b]
Gran# (× 10^3/µL)	3.95 ± 1.00	5.40 ± 2.00	2.85 ± 0.00	1.00 ± 0.00	0.00-2.66 [b]
Lymph%	12.20 ± 2.00	24.80 ± 16.00	25.20 ± 6.00	36.80 ± 0.00	
Mid%	29.90 ± 25.00	31.50 ± 24.00	30.15 ± 22.00	39.40 ± 0.00	
Gran%	57.90 ± 23.00	43.70 ± 8.00	44.65 ± 17.00	23.80 ± 0.00	
HGB (g/dL)	14.40 ± 1.00	12.70 ± 4.00	14.60 ± 1.00	14.80 ± 0.00	10-17
RBC (× 10^6/µL)	7.18 ± 3.00	4.62 ± 0.00	7.58 ± 2.00	9.51 ± 0.00	7-11
HCT (%)	46.40 ± 6.00	28.60 ± 0.00	46.80 ± 5.00	52.40 ± 0.00	35-52
MCV (fL)	70.80 ± 17.00	62.10 ± 0.00	49.95 ± 4.00	55.10 ± 0.00	45-55
MCH (pg)	22.40 ± 7.00	19.20 ± 0.00	20.45 ± 5.00	15.50 ± 0.00	15-18
MCHC(g/dL)	31.25 ± 2.00	31.10 ± 0.00	31.35 ± 2.00	28.20 ± 0.00	30-38
RDW-CV (%)	14.65 ± 2.00	19.60 ± 0.00	16.40 ± 1.00	19.00 ± 0.00	16-23
RDW-SD (fL)	34.45 ± 6.00	40.10 ± 0.00	35.20 ± 6.00	35.70 ± 0.00	
PLT (× 10^3/µL)	379.50 ± 194.00	440.00 ± 9.00	477.00 ± 287.00	740.00 ± 0.00	900-1600
MPV (fL)	6.85 ± 1.00	7.20 ± 1.00	7.80 ± 2.00	5.90 ± 0.00	4-6
RDW (%)	15.25 ± 1.00	15.50 ± 1.00	15.35 ± 0.00	15.10 ± 0.00	11-14 or 16-23[a]
PCT (%)	0.24 ± 0.00	0.32 ± 0.00	0.32 ± 0.00	0.44 ± 0.00	0.36-0.96

*: Significant differences from negative control group * (p<.05), ** (p<.01), and *** (p<.001) WBC: White Blood Cells; Lymph: Lymphocytes; Mid: Other types of white blood cells; Gran: Granulocytes; HGB: Haemoglobin; RBC: Red Blood Cells; HCT: Haematocrit; MCV: Mean Cell Volume; MCH: Mean Cell Haemoglobin; MCHC: Mean Cell Haemoglobin Concentration; RDW: Red cell Distribution Width; PLT: Platelet count; MPV: Mean Platelet Volume; PCT: Plateletcrit; NC: Negative Control. Normal ranges were obtained from The Mouse in Biomedical Research, Volume 3, Second Edition (Ihedioha, 2012; E. Everds, 2007).

Table 4 below presents the results of the hematological analysis conducted on mice administered the lowest dose (0.07 mg/kg) of sample B2.

Table 4: Summary of haematological values of mice given sample B2 and negative control (NC) for 28 days.

Parameters	B2 - 0.07mg/kg	NC	Normal range
WBC (× 10^3/µL)	5.80 ± 3.00	4.20 ± 0.00	2-10
Lymph# (× 10^3/µL)	2.00 ± 1.00	1.50 ± 0.00	2.88-11.15[b]
Mid# (× 10^3/µL)	2.15 ± 2.00	1.70 ± 0.00	0.43-3.64 [b]
Gran# (× 10^3/µL)	1.65 ± 0.00	1.00 ± 0.00	0.00-2.66 [b]
Lymph%	38.65 ± 9.00	36.80 ± 0.00	
Mid%	27.85 ± 19.00	39.40 ± 0.00	
Gran%	33.50 ± 10.00	23.80 ± 0.00	
HGB (g/dL)	15.20 ± 1.00	14.80 ± 0.00	10-17
RBC (× 10^6/µL)	7.50 ± 2.00	9.51 ± 0.00	7-11
HCT (%)	47.10 ± 2.00	52.40 ± 0.00	35-52
MCV (fL)	66.55 ± 17.00	55.10 ± 0.00	45-55
MCH (pg)	21.55 ± 6.00	15.50 ± 0.00	15-18
MCHC(g/dL)	32.20 ± 1.00	28.20 ± 0.00	30-38
RDW-CV (%)	15.90 ± 3.00	19.00 ± 0.00	16-23
RDW-SD (fL)	34.80 ± 5.00	35.70 ± 0.00	
PLT (× 10^3/µL)	417.00 ± 315.00	740.00 ± 0.00	900-1600
MPV (fL)	7.40 ± 1.00	5.90 ± 0.00	4-6
RDW (%)	15.20 ± 1.00	15.10 ± 0.00	11-14 or 16-23[a]
PCT (%)	0.27 ± 0.00	0.44 ± 0.00	0.36-0.96

*: Significant differences from negative control group * (p<.05), ** (p<.01), and *** (p<.001) WBC: White Blood Cells; Lymph: Lymphocytes; Mid: Other types of white blood cells; Gran: Granulocytes; HGB: Haemoglobin; RBC: Red Blood Cells; HCT: Haematocrit; MCV: Mean Cell Volume; MCH: Mean Cell Haemoglobin; MCHC: Mean Cell Haemoglobin Concentration; RDW: Red cell Distribution Width; PLT: Platelet count; MPV: Mean Platelet Volume; PCT: Plateletcrit; NC: Negative Control. Normal ranges were obtained from The Mouse in Biomedical Research, Volume 3, Second Edition (Everds, 2007).

[a:] Red blood cell distribution width values are inconsistent among different instruments. in part because instruments use different formulas in the calculation of this parameter. [b] :Reference values obtained from a study conducted by Ihedioha et al., 2012 (Ihedioha *et al*., 2012).

HISTOPATHOLOGICAL EXAMINATION

The results of the histopathological examination carried out on selected organs of the mice administered sample A1 and A2 are given in the table below.

Table 5: Histopathological findings on the heart at the end of the 28-day intraperitoneal administration of Sample A1.

Organ	Histopathological Finding	Treatment			
		Negative control	A1 0.07mg/kg	A1 0.20mg/kg	A1 0.60mg/kg
Heart	Vascular congestion	-	-	-	++
	Cardiac edema	-	-	-	++
	Mononuclear infiltrates	-	-	-	++
Kidney	Vascular congestion	-	-	-	+
	Renal edema	-	-	-	-
Liver	Vascular congestion	-	+	++	+++
	Hepatic edema	-	+	++	-
		Negative control	A2 0.07mg/kg	A2 0.20mg/kg	A2 0.60mg/kg
Heart	Vascular congestion	-	-	++	-
	Cardiac edema	-	-	-	-
	Mononuclear infiltrates	-	-	++	-
Kidney	Vascular congestion	-	-	-	-
	Renal edema	-	-	-	-
Liver	Vascular congestion	-	+	++	+++
	Hepatic edema	-	-	+	-

– absent, + mild, ++ moderate and +++ severe vascular congestion accompanied with mononuclear infiltrates and/or edema

The results of the histopathological examination carried out on selected organs of the mice administered sample B1 and B2 are given in the table below.

Table 6: Histopathological findings on the heart at the end of the 28-day intraperitoneal administration of Samples B1 and B2, and pretreatment samples PTA1, PTA2 and PTB1.

Organ	Histopathological Finding	Treatment			
		Negative control	B1 0.07mg/kg	B1 0.20mg/kg	B1 0.60mg/kg
Heart	Vascular congestion	-	-	++	+++
	Cardiac edema	-	-	-	+
	Mononuclear infiltrate	-	-	++	-
Kidney	Vascular congestion	-	-	-	+
	Renal edema	-	-	-	+
Liver	Vascular congestion	-	+	++	+++
	Hepatic edema	-	+	-	+++
		Negative control	B2 0.07mg/kg		
Heart	Vascular congestion	-	+++		
	Cardiac edema	-	+++		
	Mononuclear infiltrates	-	+++		
Kidney	Vascular congestion	-	+		
	Renal edema	-	+		
Liver	Vascular congestion	-	++		
	Hepatic edema	-	++		
		Negative control	PTA1 0.71mg/kg	PTA2 0.71mg/kg	PTB1 0.71mg/kg
Heart	Vascular congestion	-	++	-	+
	Cardiac edema	-	-	-	+
	Mononuclear filtrates	-	++	-	+
Kidney	Vascular congestion	-	-	+	++
	Renal edema	-	-	-	++
Liver	Vascular congestion	-	++	++	++
	Hepatic edema	-	++	++	++

– absent, + mild, ++ moderate and +++ severe vascular congestion accompanied with mononuclear infiltrates and/or edema.

COMPUTATIONAL IMAGE ANALYSIS

A representative photomicrograph of tissue cross section as shown in Figure 4 below, annotated Bowman's capsule and a sample output of the automatic detection of the Bowman's space and glomeruli.

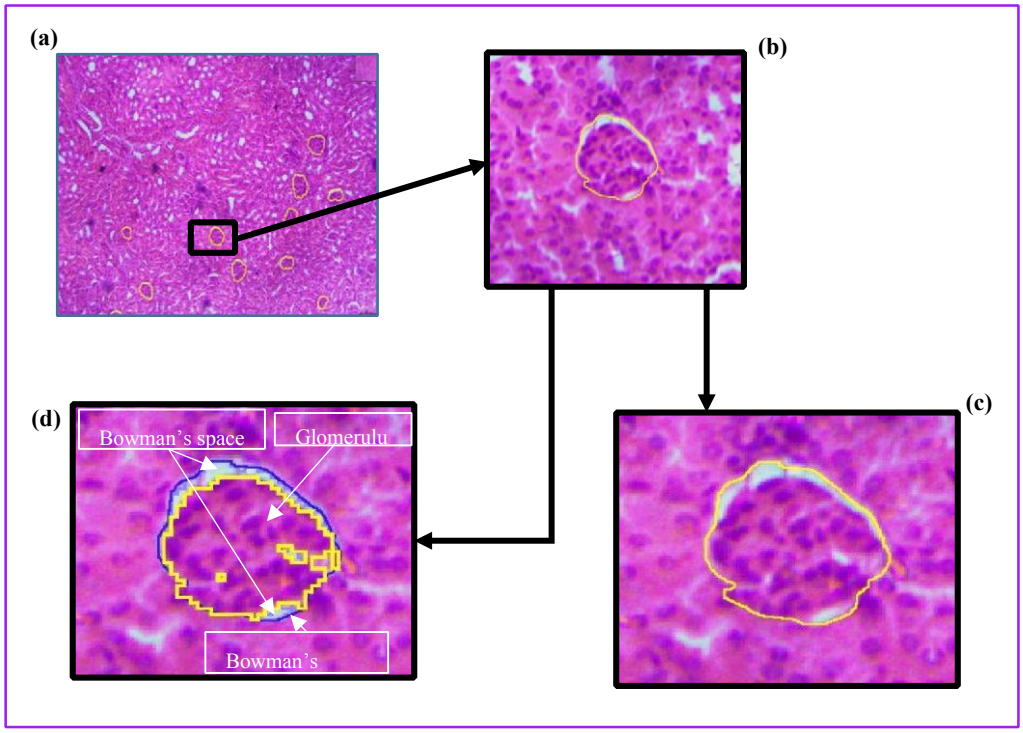

Figure 4: Representative images of H & E kidney tissue cross-section at different zoom levels (H&E, X100). (a) A kidney cross-section showing annotated glomeruli indicated by the annotated polygons; scale bar: 100 µm (b) An enlarged image of the kidney cross section showing a single Bowman's capsule; scale bar: 50 µm. (c) A single annotated Bowman's capsule with tubules in the background; scale bar: 20 µm. (d) An image generated by computational analysis showing an annotated Bowman's capsule (indicated by the Polyline), the glomerulus (yellow polygon), and empty spaces between the region of annotation (in blue) which represent the Bowman's space.

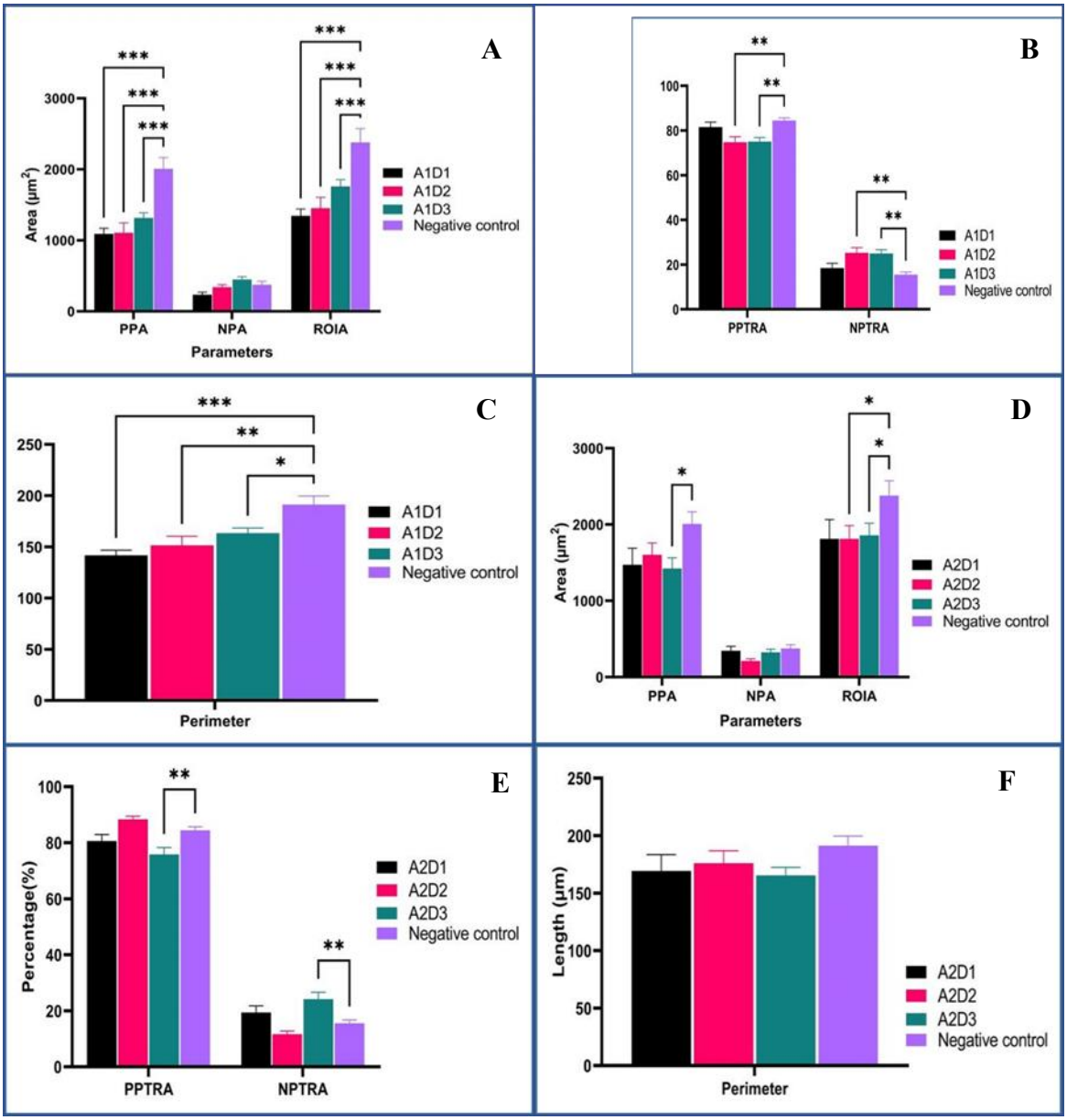

Figure 5: Comparative analysis of sample A1 (A, B and C) and sample A2 (D, E and F) treatment effects on mouse kidney: positive pixel area (PPA), region of interest area (ROIA), positive percentage of total region of interest area (PPTRA) and negative percentage of total region of interest area (NPPTRA) and bowman's capsule perimeter.

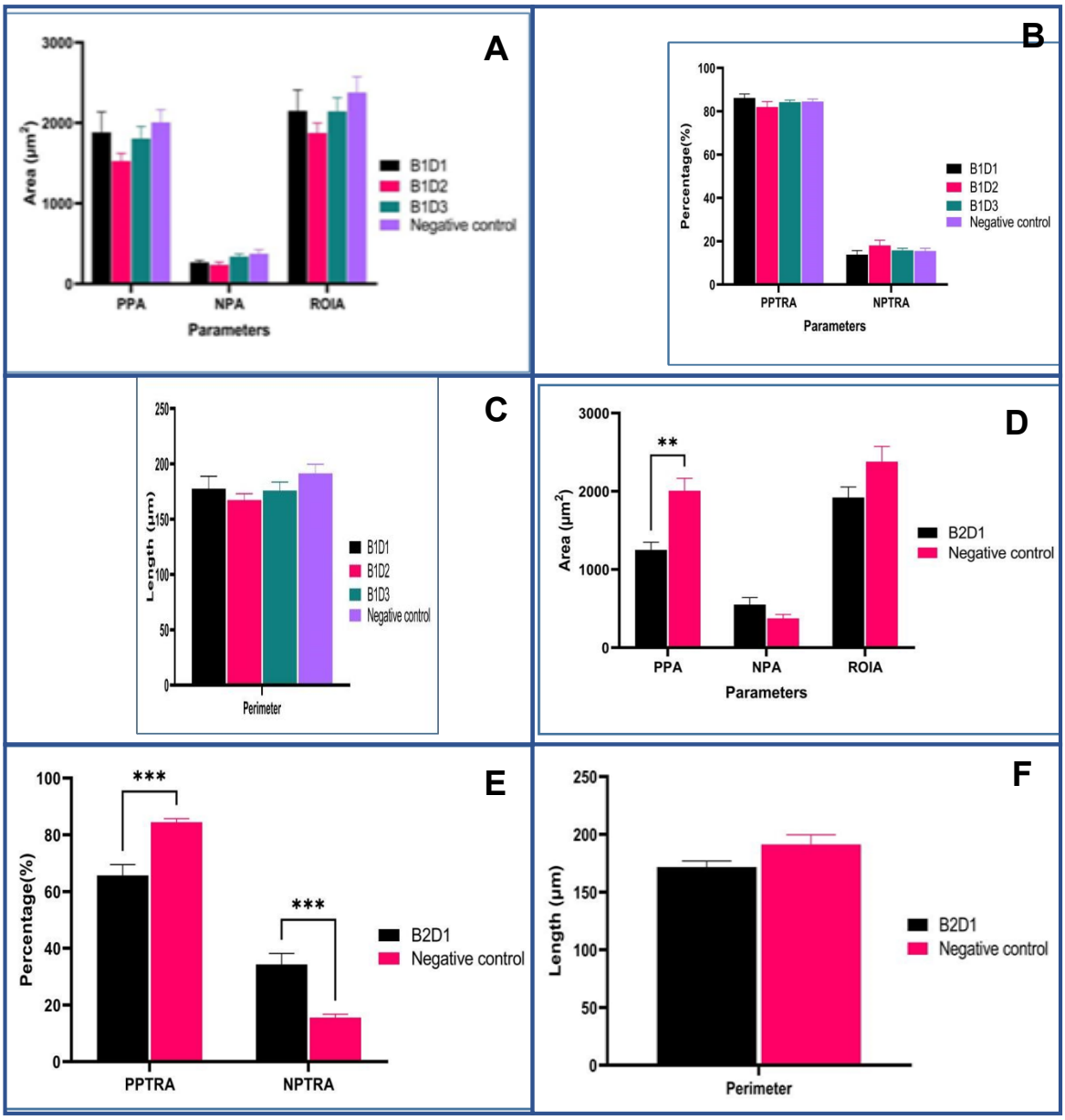

Figure 6: Comparative analysis of sample B1 (A, B, and C) and sample B2 (D, E, and F) treatment effects on mouse kidney: positive pixel area (PPA), region of interest area (ROIA), positive percentage of the total region of interest area (PPTRA) and negative percentage of the total region of interest area (NPPTRA) and bowman's capsule perimeter.

DISCUSSION

Ultraviolet-visible spectroscopic analysis indicated that compound A1 showed transitions around 266– 275 nm attributed to π-π* and B1 exhibited transitions around 345 nm attributed to n-π^*. These transitions can be attributed to C=C as well as localized surface plasmon resonance (LSPR) band in the compounds characteristics of silver nanoparticles usually found between 345 – 450 nm and the presence of hetero atoms such as nitrogen in B1.

Meanwhile, the infrared spectra reveal bands in the region of 1633-1637 cm^{-1} attributed to H_2C=NH and the presence of coordinated water is indicated by a band in the region 3625–3897 cm^{-1}. The presence of CH stretching frequency in alkanes was confirmed by bands around 2320–2351 cm^{-1}. A strong band around 1383 and 1384 cm^{-1} observed in Figures 1C and 1D is attributed to NO_2 stretch. The bands in the spectra around 666–674 cm^{-1} are allotted to frequency stretching of (Ag-O from AgO^{2-}) bond formation, confirming the bio-reduction of $AgNO_3$ to elemental Ag^0 forming AgNPs. Similar results were reported by Sivaraj *et al*. 2014 and Ahmad *et al*. 2019.

The results of the TEM images indicate that the materials were spherical in shape with an average size in the range of 240 nm. Non-uniform spherical images were captured by the TEM micrograph of the nanomaterials as shown in Figure 1G and H. The TEM micrographs indicated that the materials did not agglomerate, which complements the SEM results (Figure 1E, and F) in this study.

Pre-treatment toxicity results of the single dose of 0.71 mg/kg of samples A1, A2, B1 and B2 on mice labelled as PTA1, PTA2, PTB1 and PTB2 respectively showed that the B2 sample PTB2) was the most toxic as depicted in the histopathological results images in Table 6. The pre-treated animals did not recover from the administered dose with the exception of PTA1, which had a normal kidney and PTA2 which had a normal heart. The PTB2 group died within 72 hours of receiving the dose. This resulted further guided the dose(s) selection in the subsequent subacute toxicity study.

During the subacute toxicity study, body weight examination was carried out on mice which received daily intraperitoneal doses of extracts of seed and shell of *Abrus precatorius* and its biosynthesized nanoparticles. According to Porwal *et al*. 2017 and Zhang *et al*. 2021, both reduction and increase in the body weight are important indicators in assessing the toxicity of a test sample (Zhang *et al*. 2021; Porwal *et al*. 2017). The marked decrease in body weight (results not included) observed in the highest and mid dose of the *Abrus precatorius* seed sample (sample B2) group before their eventual death within the first week could be due to the loss of appetite following the administration of the test sample leading to the loss of adipose tissue or muscle wasting (Srivastava *et al*. 2021; Mughal *et al*. 2021; Baxi *et al*. 2022). From a previous study on the intraperitoneal administration of aqueous extract of *Abrus precatorius* seeds on rats, there was a significant decrease in the body weight of test animals which received 0.20 mg/kg of the test sample when compared with the control; no mortality was observed at this dose for 14 days (Sunday *et al*. 2013). Perhaps due to the less toxic nature of the *Abrus precatorius* shell as compared with the seed (Madabhushi and Lee. 2016; Emon *et al.* 2021), the reduced toxicological response was evident in the biosynthesized nanoparticles of the plant part. The test animals treated with the seed shell mediated nanoparticles (sample A1) showed a generally less significant change in weight when compared with the seed-mediated nanoparticles (sample B1). The general increase in the body weight of the test animals could confirm research conducted by Niyogi and Rieders which stated that mice could develop tolerance to the toxic principles of *Abrus precatorius* (Tang *et al*. 2020). Photomicrographs of the histopathological examination of the heart, liver and kidney sections (not included) of the non-surviving animals showed severe vascular congestion of the heart, liver and the kidney, cortical haemorrhage of the kidney and edema especially in the liver and the heart highlighting the toxicity of the B2 sample at these doses. As indicated by Table 1 and Table 2, and likewise illustrated by Figures 2 and 3, A2 and B1 treatment group both had an increase in platelet number as the doses increased which means that both samples could either stimulate platelet production (Nurden and Nurden, 2020) or this could be a sign of inflammation which often leads to increased platelet count (Qian *et al*. 2020; Romandini *et al*. 2018). As indicated in Table 1 and Table 2, the A2 and B1 treatment group both had an increase in platelet number as the doses increased which means that both samples could either stimulate platelet production (Nurden and Nurden. 2020) or this could be a sign of inflammation which often leads to increased platelet count (Romandini *et al*. 2018; Qian *et al.* 2020). It was also observed that granulocyte percentage (Gran%) increased with increase in the dose in sample A1 as illustrated in Figure 2C.

An increase in the percentage of granulocytes (neutrophil being the most abundant (Rosales, 2018; O'connell *et al.* 2015) has recently been associated with liver impairment, disease or inflammation (Tang *et al*. 2021; Cho and Szabo. 2021); this further corroborates the result of the histopathological result given in Table 5 which showed an increase in the extent of hepatic vascular congestion with increasing dose. As shown in Figure 2, there was a dose related increase in the mean cell volume (MCV) in the sample A1 treatment groups, however, the difference between MCV between the mid dose (0.20mg/kg) and the highest dose (0.60 mg/kg) was less than one femtolitre. Figures 2 and 3 indicate that with increasing dose of samples A2 and B1, there was a complimentary reduction in an initially very high MCV as compared with the negative control and the normal range; this could indicate a gradual correction of a likely macrocytic anaemia with increasing dose, or correction of iron deficiency due to the high iron content in samples A2 and B1 (Chakradhari *et al.* 2019). It was also observed that there was a dose dependent decline in the values of RBC (red blood cell count), haematocrit (HCT) and hemoglobin (HGB) in samples A2 and A1 according to Figures 2 implying a likely condition of anaemia (Pisulkar *et al.* 2021) or a damage to the liver as suggested by the photomicrographs of liver sections of both sample A1 and A2 in Figures 19 and 21 (Xie *et al*. 2016; Yang *et al*. 2018).

Since HGB and HCT values are indicative of anaemia therefore, the result shown in Figures 2F and 2C shows that there is an increase in anaemic tendency with increase in the doses of samples A2 and A1 respectively: RBC (red blood cell count) and haematocrit (HCT), were lower in the B2 treatment group as compared with the negative control. In all the treatment groups, and at all doses except in the highest dose of B1 (0.60 mg/kg) (Table 3) and lowest dose of A1 as shown in Table 1, the values of the mean cell volume were higher when compared with the negative control group and the normal range (E. Everds 2007); this could indicate a form of anaemia called macrocytic anaemia in which the average size of the red blood cells are larger than normal; this abnormal size could be due to nutrient deficiency (Newhall *et al*. 2020; Kujovich 2016) or a liver impairment (Yang *et al*. 2018; Zhao *et al*. 2021). The latter is highly likely due to the increasing severity of vascular congestion with increasing dose observed in the

histopathological examination of the liver of the treatment groups as shown in Tables 5 and 6.

However, at the highest dose of sample A1 (0.60 mg/kg), there was approximately 15% decrease in the number of lymphocytes when compared with the mid dose and the lowest dose which were of equal values; this suggests that at higher doses sample A1 could also cause lymphopenia. The platelet count of sample A1 mid dose and highest dose treatment groups were far lower than the negative control treatment groups suggesting thrombocytopenia and this could be due to a condition liver impairment or fibrosis (Cai *et al*. 2018; Karagoz *et al*. 2014). More so, the liver is the site of the production of thrombopoietin (a hormone which regulates platelet production) (Kuter 2013). The observed thrombocytopenia (decreased platelet count) could also be as result of the destruction of platelets and circulation of premature and large platelets as suggested by the high mean platelet volume (Benlachgar *et al.*, 2020; Gulati *et al.*, 2017). As shown in Table 1, the WBC (white blood cells) and Lymph# (lymphocyte number) of the lowest dose treatment group of the A1 sample were higher than the negative control group; this suggests inflammation which could lead to widespread organ damage (Chen *et al*. 2018; Ernandez and Mayadas. 2016). The results of histopathological examination shown in Table 6 confirm a likely inflammation in the surviving B2 treatment group (0.07 mg/kg) more so all the selected organs had both vascular congestion and edema, and the heart photomicrographs had mononuclear infiltrates. The histopathological examination of the animals which received 0.71 mg/kg single intraperitoneal dose of the treatment samples at the start of the study still showed signs of hepatotoxicity at the end of the study as illustrated in Table 6. Also, Table 5 showed that the A1-treated animal had a normal kidney and also demonstrated that the A2- treated animal had a normal heart, this further corroborated the result of the repeated-dose subacute toxicity study which suggested that the most susceptible organ to toxicity for the treatment samples was the liver-confirming its role as the primary site of biotransformation of xenobiotics (Beyerle *et al*. 2015; Lindamood. 2020). Meanwhile, liver is a major organ involved in the accumulation, processing and clearance of nanoparticles from the body (Campbell *et al*. 2018; Tsoi *et al*. 2016). The presence of mononuclear filtrates in the heart micrographs of the highest dose of A1, the mid dose of A2 and B1, the highest dose of B1 and in the least dose of sample of B2 shows that at sufficiently high doses, all the treatment samples could cause an inflammation of the myocardium. This result is consistent with results of previous research studies on parts of *Abrus precatorius* which indicated myocarditis and cardiomyopathy (Saganuwan *et al*. 2011; Saganuwan *et al*. 2014; Maregesi *et al*. 2016; Tion *et al*. 2018). In recent times, there has been attempts to interpret photomicrographs of tissues obtained from microscope camera with special imaging softwares which are able to accurately detect and measure morphological and structural features of digital images of tissue sections.

The results of digital morphometry of the Bowman's capsule, Bowman's space and glomeruli in this study indicated that upon the administration of sample A1, there was a dose-related increase in the Bowman's capsule's area as shown in Figure 5, the area increased from 1344.93 ± 98.34 μm^2 at the least dose (0.07mg/kg) to 1759.93 ± 95.70 μm^2 at the highest dose (0.60 mg/kg). The measurements were significantly lower at $p<.001$ implying that the Bowman's capsule of the mice treated with sample A1 were significantly smaller in size when compared with the negative control. Meanwhile, the area of the Bowman's space was not significantly different from the negative control. The percentage of the glomerulus in the Bowman's capsule (PPTRA) according to Figure 5B shows that the mid and high dose groups of sample A1 had glomeruli that were moderately larger in comparison with their Bowman's capsule than the negative control at $p<.01$. This could imply an instance of glomerular hypertrophy which could be as a result of an enlargement of the glomerular capillary due to hyperfiltration (Helal *et al*. 2012; Cortinovis *et al*. 2022).

Figure 5E also shows that the Bowman's space is moderately significantly higher in the sample A1 mid dose and high dose than the negative control, this indicates an enlargement of the Bowman's space as a result of an increase in flow into the Bowman's space due to hyperfiltration (Tobar *et al*. 2013; Chagnac *et al*. 2019). Similarly, Figure 5C shows that the perimeter of the Bowman's capsule increases with the increase in dose of sample A1 and it confirms the earlier measurement of area. Just like the area of the Bowman's capsule, the perimeter of the Bowman's capsule in the mice administered sample A1 increased by approximately 6% when the dose was increased to 0.20 mg/kg and by approximately 13% when increased to the highest dose (0.60 mg/kg). This shows that sample A1 has a dose-dependent effect on the size of both the Bowman's capsule, Bowman's space and the glomerulus. Sales *et al*., reported that drugs such as amphotericin B, polymyxins, and tenofovir could adversely affect the Bowman's capsule (Sales and Foresto. 2020). Figure 5D shows that the size of the glomerulus (PPA) is significantly different at $p<.05$ for the highest dose of sample A2 (0.60 mg/kg) when compared with the negative control. Also, the size of the Bowman's capsule for the mice administered the mid dose and the highest dose of sample A2 had a statistically smaller size of glomerulus at $p<.05$. The highest dose of sample A2 had both the significantly different fraction of glomerulus and Bowman's space which were 75.85 ± 2.48 and 24.15 ± 2.48 respectively according to Figure 5E. This result implies that at a dose of 0.60 mg/kg, sample A2 could reduce the size of glomerulus significantly and thereby increase the size of Bowman's space causing glomerular atrophy such as reported by Mohamed *et al*. in their study on the doxorubin-induced nephrotoxicity suppression study (Mohamed *et al*. 2022). Collapsing glomerulopathy has been found to be induced by pamidronate or other drugs which could inhibit pathways essential for cell differentiation such as mevalonate synthesis pathway (Markowitz *et al*. 2015). From Figure 5F, the perimeter of the Bowman's capsule of the treated animals were found to be insignificantly different from the negative control. As illustrated in Figures 6A, 6B and 6C, none of the measured parameters showed a significant difference from the negative control. However, the charts show that the mid dose of sample B1 (0.20 mg/kg) had a smaller size of glomerulus when compared with the mid dose and the high dose but a slightly higher percentage of Bowman's space. The result shows that the Bowman's capsules of sample B1 treatment group had no measurable glomerulopathy in terms of the measured parameters of Bowman's capsule perimeter and area, glomerular area, Bowman's space, percentage of the Bowman's space and percentage of glomerular area. The only surviving dose group of sample B2 had a considerably lower glomerular area and Bowman's capsule area when compared with the negative control as seen in Figures 6D and 6E. Figure 6E shows that mice administered the lowest dose of B2 had a higher percentage of Bowman's space as a fraction of its Bowman's capsule as compared with the negative control, this confirms a likely glomerulopathy associated with glomeruli atrophy, or collapsing glomerulopathy.

CONCLUSION

This study shows that intraperitoneally-administered biosynthesized nanoparticles from parts of *Abrus precatorius* (seed and seed husk) had significantly lower toxicity than the crude extracts and therefore these nanoparticles could be used as less toxic or safer alternative to assess the various pharmacological activities and medicinal effects of the plant parts as shown by the results of histopathological examination. More so, no mortality was recorded in the biosynthesized nanoparticle treatment groups as compared with the crude extracts. However, the study illustrated that the most affected organ in terms of toxicity among the selected target organs is the liver followed by the while the least affected was the kidney.

Therefore, doses lower than 0.07 mg/kg of *Abrus precatorius* seed shell mediated nanoparticles and crude shell and seed of *Abrus precatorius* have less potential of altering the morphology of the Bowman's capsule and therefore less likely to cause a loss of renal function.

REFERENCES

Ahmad, S., Munir, S., Zeb, N., Ullah, A., Khan, B., Ali, J., Bilal, M., Omer, M., Alamzeb, M. and Salman, S. M. (2019) "Green nanotechnology: A review on green synthesis of silver nanoparticles—An ecofriendly approach." *International journal of nanomedicine*, 5087-5107.

Arif, E. and Nihalani, D. (2013) "Glomerular Filtration Barrier Assembly: An insight."*Postdoc J,*1, 33-45.

Baxi, V., Edwards, R., Montalto, M. and Saha, S. (2022) "Digital pathology and artificial intelligence in translational medicine and clinical practice."*Mod Pathol,* 35, 23-32.doi:10.1038/s41379-021-00919-2.

Benlachgar, N., Doghmi, K., Masrar, A., Mahtat, E. M., Harmouche, H. and Mezalek, Z. T. (2020). Immature platelets: a review of the available evidence. *Thrombosis research,* 195, 43-50.

Beyerle, J., Frei, E., Stiborova, M., Habermann, N. and Ulrich, C. M. (2015) "Biotransformation of xenobiotics in the human colon and rectum and its association with colorectal cancer." *Drug metabolism reviews,* 47, 199-221.

Cai, J., Wang, K., Han, T. and Jiang, H. (2018) "Evaluation of prognostic values of inflammation-based makers in patients with HBV-related acute-on-chronic liver failure." *Medicine,* 97.

Campbell, F., Bos, F. L., Sieber, S., Arias-Alpizar, G., Koch, B. E., Huwyler, J., Kros, A. and Bussmann, J. (2018) "Directing Nanoparticle Biodistribution through Evasion and Exploitation of Stab2-Dependent Nanoparticle Uptake." *ACS Nano,* 12, 2138-2150. doi:10.1021/acsnano.7b06995.

Carmona, E. R., Benito, N., Plaza, T. and Recio-Sánchez, G.(2017) "Green synthesis of silver nanoparticles by using leaf extracts from the endemic Buddleja globosa hope." *Green Chemistry Letters and Reviews,* 10, 250-256.

Chagnac, A., Zingerman, B., Rozen-Zvi, B. and Herman-Edelstein, M. (2019) "Consequences of Glomerular Hyperfiltration: The Role of Physical Forces in the Pathogenesis of Chronic Kidney Disease in Diabetes and Obesity." *Nephron,* 143, 38-42. doi:10.1159/000499486.

Chambers, B. E., Clark, E. G., Gatz, A. E. and Wingert, R. A. (2020) "Kctd15 regulates nephron segment development by repressing Tfap2a activity." *Development,* 147, dev191973. doi:10.1242/dev.191973.

Chantler, C. and Holliday, M. (1987) "Progressive loss of renal function." *Pediatric nephrology,* 2.

Chen, L., Deng, H., Cui, H., Fang, J., Zuo, Z., Deng, J., Li, Y., Wang, X. and Zhao, L. (2018) "Inflammatory responses and inflammation-associated diseases in organs." *Oncotarget,* 9, 7204-7218. doi:10.18632/oncotarget.23208.

Chen, L. and Liang, J. (2020) "An overview of functional nanoparticles as novel emerging antiviral therapeutic agents." *Materials Science and Engineering: C,* 112, 110924.

Cheng, W., Zhao, X., Luo, W., Zhang, Y., Wang, Y. and Fan, G. (2020) "Bagasse□derived Carbon□ supported Ru nanoparticles as Catalyst for Efficient Dehydrogenation of Ammonia Borane." *ChemNanoMat,* 6, 1251-1259.

Cho, Y. and Szabo, G. (2021) "Two Faces of Neutrophils in Liver Disease Development and Progression." *Hepatology,* 74, 503-512. doi: 10.1002/hep.31680.

Clark, W. R., Dehghani, N. L., Narsimhan, V. and Ronco, C. (2019) "Uremic toxins and their relation to dialysis efficacy." *Blood Purification,* 48, 299-314.

Cortinovis, M., Perico, N., Ruggenenti, P., Remuzzi, A. and Remuzzi, G. (2022) "Glomerular hyperfiltration." *Nature Reviews Nephrology,* 18, 435-451. doi:10.1038/s41581-022-00559-y.

Das, P. E., Abu-Yousef, I. A., Majdalawieh, A. F., Narasimhan, S. and Poltronieri, P. (2020) "Green Synthesis of Encapsulated Copper Nanoparticles Using a Hydroalcoholic Extract of Moringa oleifera Leaves and Assessment of Their Antioxidant and Antimicrobial Activities." *Molecules,* 25. doi:10.3390/molecules25030555.

Eeverds, N. (2007). Hematology of the Laboratory Mouse. *In:* FOX, J. G., DAVISSON, M. T., QUIMBY, F. W., BARTHOLD, S. W., NEWCOMER, C. E. & SMITH, A. L. (eds.) *The Mouse in Biomedical Research.* Burlington: Academic Press, 133-170.

Emon, M. U., Islam, R., Keya, M. S. and Zannat, R. (2021) Performance Analysis of Chronic Kidney Disease through Machine Learning Approaches. 6th International Conference on Inventive Computation Technologies (ICICT). IEEE, 713-719.

Ernandez, T. and Mayadas, T. N. (2016) "The Changing Landscape of Renal Inflammation." *Trends Mol Med,* 22, 151-163. doi:10.1016/j. molmed.2015.12.002.

Gnatowski, A., Martín-Ramos, P., Towett, E. K., Patel, K. S. and Chakradhari, S. (2019) "Chemical Composition of *Abrus precatorius* L. Seeds." *European Journal of Medicinal Plants,* 28, 1-6. doi:10.9734/ejmp/2019/v28i130125.

Gulati, I., Kumar, H., Sheth, J. and Dey, I. (2017) "Diagnostic implication of mean platelet volume in thrombocytopenia." *Medical Journal of Dr. DY Patil University,* 10, 370.

Helal, I., Fick-Brosnahan, G. M., Reed-Gitomer, B. and

Schrier, R. W. (2012) "Glomerular hyperfiltration: definitions, mechanisms and clinical implications." *Nature Reviews Nephrology,* 8, 293-300. doi:10.1038/nrneph.2012.19.

Ihedioha, J., J.I, U., Agina, O., Udeani, I. and Daniel-Igwe, G. (2012) "Reference values for the haematology profile of conventional grade outbred albino mice (Mus musculus) in Nsukka, Eastern Nigeria." *Animal Research International,* 9, 1601-1612.

Jorge De Souza, T. A., Rosa Souza, L. R. and Franchi, L. P. (2019) "Silver nanoparticles: An integrated view of green synthesis methods, transformation in the environment, and toxicity." *Ecotoxicol Environ Saf,* 171, 691-700. doi:10.1016/j.ecoenv.2018.12.095.

Karagoz, E., Ulcay, A., Tanoglu, A., Kara, M., Turhan, V., Erdem, H., Oncul, O. and Gorenek, L.(2014) "Clinical usefulness of mean platelet volume and red blood cell distribution width to platelet ratio for predicting the severity of hepatic fibrosis in chronic hepatitis B virus patients." *European journal of gastroenterology & hepatology,* 26, 1320-1324.

Kujovich, J. L. (2016) "Evaluation of Anemia." *Obstet Gynecol Clin North Am,* 43, 247-64. doi:10.1016/j.ogc.2016.01.009.

Kuter, D. J. (2013) "The biology of thrombopoietin and thrombopoietin receptor agonists." *International Journal of Hematology,* 98, 10-23. doi:10.1007/s12185-013-1382-0.

Larayetan, R., Ojemaye, M. O., Okoh, O. O. and Okoh, A. I. (2019) "Silver nanoparticles mediated by *Callistemon citrinus* extracts and their antimalaria, antitrypanosoma and antibacterial efficacy." *Journal of Molecular Liquids,* 273, 615-625.

Lindamood, C. (2020). Xenobiotic biotransformation. *Hepatotoxicology.* CRC Press, 139-180.

Madabhushi, A. and Lee, G. (2016) "Image analysis and machine learning in digital pathology: Challenges and opportunities." *Med Image Anal,* 33, 170-175. doi:10.1016/j.media.2016.06.037.

Maregesi, S. M., Mwakigonja, A. R. and Urio, P. (2016) "Toxicity evaluation of *Abrus precatorius* seeds collected from Bunda District, Tanzania." *Sch Acad J Pharm,* 5, 399-405.

Markowitz, G. S., Bomback, A. S. and Perazella, M. A. (2015) "Drug-induced glomerular disease: direct cellular injury." *Clin J Am Soc Nephrol,* 10, 1291-9. doi:10.2215/cjn.00860115.

Mohamed, H. K., Mobasher, M. A., Ebiya, R. A., Hassen, M. T., Hagag, H. M., El-Sayed, R., Abdel-Ghany, S., Said, M. M. and Awad, N. S. (2022) "Anti-Inflammatory, Anti-Apoptotic, and Antioxidant Roles of Honey, Royal Jelly, and Propolis in Suppressing Nephrotoxicity Induced by Doxorubicin in Male Albino Rats." *Antioxidants,* 11, 1029.

Mughal, B., Zaidi, S. Z. J., Zhang, X. and Hassan, S. U. (2021) "Biogenic nanoparticles: Synthesis, characterisation and applications." *Applied Sciences,* 11, 2598.

Newhall, D., Oliver, R.and Lugthart,S. (2020)"Anaemia: A disease or symptom."*Neth. J. Med,*78,104-110.

Nurden, A. T. and Nurden, P. (2020) "Inherited thrombocytopenias: history, advances and perspectives." *Haematologica,* 105, 2004-2019. doi:10.3324/haematol.2019.233197.

O'connell, K. E., Mikkola, A. M., Stepanek, A. M., Vernet, A., Hall, C. D., Sun, C. C., Yildirim, E., Staropoli, J. F., Lee, J. T. and Brown, D. E. (2015) "Practical murine hematopathology: a comparative review and implications for research." *Comp Med,* 65, 96-113.

Ojemaye, M. O., Okoh, S. O. and Okoh, A. I. (2021). "Silver nanoparticles (AgNPs) facilitated by plant parts of Crataegus ambigua Becker AK extracts and their antibacterial, antioxidant and antimalarial activities." *Green Chemistry Letters and Reviews,* 14, 51-61.

Pisulkar, S. K., Dahihandekar, C., Sathe, S., Godbole, S. and Pisulkar, G. (2021) "Prosthetic Rehabilitation of a Patient with Symptoms of Iron Deficiency Anaemia in association with Fraser's Syndrome–A Case Report." *Indian Journal of Forensic Medicine & Toxicology,* 15, 518-522.

Porwal, M., Khan, N. A. and Maheshwari, K. K. (2017) "Evaluation of Acute and Subacute Oral Toxicity Induced by Ethanolic Extract of Marsdenia tenacissima Leaves in Experimental Rats." *Sci Pharm,* 85, 29. doi:10.3390/scipharm85030029.

Qian, H., Chen, R., Wang, B., Yuan, X., Chen, S., Liu, Y. and Shi, G. (2020) "Associations of Platelet Count with Inflammation and Response to Anti-TNF-alpha Therapy in Patients with Ankylosing Spondylitis." *Front Pharmacol,* 11, 559593. doi:10.3389/fphar.2020.559593.

Rao, P. V. and Gan, S. H. (2015) "Recent Advances in Nanotechnology-Based Diagnosis and Treatments of Diabetes." *Curr Drug Metab,* 16, 371-5. doi:10.2174/1389200215666141125120215.

Romandini, M., Lafori, A., Romandini, P., Baima, G. and Cordaro, M. (2018) "Periodontitis and platelet count: A new potential link with cardiovascular and other systemic inflammatory diseases." *J Clin Periodontol,* 45, 12991310. doi:10.1111/jcpe.13004.

Rosales, C. (2018) "Neutrophil: A Cell with Many Roles in Inflammation or Several Cell Types?" *Front Physiol,* 9, 113. doi:10.3389/fphys.2018.00113.

Saganuwan, S. A., Onyeyili, P. A., Ameh, E. G. and Udok Etuk, E. (2011) "In vivo antiplasmodial activity by aqueous extract of *Abrus precatorius* in mice." *Revista latinoamericana de química,* 39, 32-44.

Saganuwan, S. A., Onyeyili, P. A. and Etuk, E. U. (2014) "Immuno modulatory potentials and histopathological effects of aqueous extract of *Abrus precatorius* leaf in mus musculus." *Journal of Hematology Research,* 1, 5462.

Sales, G. T. M. and Foresto, R. D. (2020) "Drug-induced nephrotoxicity." *Revista da Associação Médica Brasileira,* 66.

Sivaraj, R., Rahman, P. K., Rajiv, P., Narendhran, S. and Venckatesh, R. (2014) "Biosynthesis and characterization of Acalypha indica mediated copper oxide nanoparticles and evaluation of its antimicrobial and anticancer activity." *Spectrochim Acta A Mol Biomol Spectrosc,* 129, 255-8. doi:10.1016/j.saa.2014.03.027.

Solomon, R. and Goldstein, S. (2017) "Real-time measurement of glomerular filtration rate." *Curr Opin Crit Care,* 23, 470-474. doi:10.1097/MCC.0000000000000456.

Srivastava, S., Usmani, Z., Atanasov, A. G., Singh, V. K., Singh, N. P., Abdel-Azeem, A. M., Prasad, R., Gupta, G., Sharma, M. and Bhargava, A. (2021) "Biological Nanofactories: Using Living Forms for Metal Nanoparticle Synthesis." *Mini Rev Med Chem,* 21, 245-265. doi:10.2174/1389557520999201116163012.

Sunday, R. M., Ilesanmi, O. and Obuotor, E. M. (2013) "Acute And Subacute Toxicity Of Aqueous Extract Of *Abrus precatorius* Seed In Wister Rats." *The Internet Journal of Pharmacology,* 11. doi:10.5580/2ce3.

Tang, C., Livingston, M. J., Liu, Z. and Dong, Z. (2020) "Autophagy in kidney homeostasis and disease." *Nat Rev Nephrol,* 16, 489-508. doi:10.1038/s41581-020-0309-2.

Tang, J., Yan, Z., Feng, Q., Yu, L. and Wang, H. (2021) "The Roles of Neutrophils in the Pathogenesis of Liver Diseases." *Frontiers in Immunology,* 12. doi:10.3389/fimmu.2021.625472.

Tecklenborg, J., Clayton, D., Siebert, S. and Coley, S. M. (2018) "The role of the immune system in kidney disease." *Clin Exp Immunol,* 192, 142-150. doi:10.1111/cei.13119.

Tion, M., Fotina, H. and Alhaji Saganuwan, S. (2018) "Phytochemical screening, proximate analysis, median lethal dose (LD50), hematological and biochemical effects of various extracts of *Abrus precatorius* seeds in Mus musculus." *Journal of Advanced Veterinary and Animal Research,* 5, 354. doi:10.5455/javar.2018.e286.

Tobar, A., Ori, Y., Benchetrit, S., Milo, G., Herman-Edelstein, M., Zingerman, B., Lev, N., Gafter, U. and Chagnac, A. (2013) "Proximal tubular hypertrophy and enlarged glomerular and proximal tubular urinary space in obese subjects with proteinuria." *PLoS One,* 8, e75547. doi:10.1371/journal.

Tsoi, K. M., Macparland, S. A., Ma, X.-Z., Spetzler, V. N., Echeverri, J., Ouyang, B., Fadel, S. M., Sykes, E. A., Goldaracena, N., Kaths, J. M., Conneely, J. B., Alman, B. A., Selzner, M., Ostrowski, M. A., Adeyi, O. A., Zilman, A., Mcgilvray, I. D. and Chan, W. C. W. (2016) "Mechanism of hard-nanomaterial clearance by the liver." *Nature Materials,* 15, 1212-1221. doi:10.1038/nmat4718.

Tsuboi, N., Okabayashi, Y., Shimizu, A. and Yokoo, T. (2017) "The Renal Pathology of Obesity." *Kidney Int Rep,* 2, 251-260. doi:10.1016/j.ekir.2017.01.007.

Turner, O. C., Aeffner, F., Bangari, D. S., High, W., Knight, B., Forest, T., Cossic, B., Himmel, L. E., Rudmann, D. G., Bawa, B., Muthuswamy, A., Aina, O. H., Edmondson, E. F., Saravanan, C., Brown, D. L., Sing, T. and Sebastian, M. M. (2020) "Society of Toxicologic Pathology Digital Pathology and Image Analysis Special Interest Group Article*: Opinion on the Application of Artificial Intelligence and Machine Learning to Digital Toxicologic Pathology." *Toxicol Pathol,* 48, 277-294. doi:10.1177/0192623319881401.

Wong, C. H., Siah, K. W. and Lo, A. W. (2019) "Estimation of clinical trial success rates and related parameters." *Biostatistics,* 20, 273-286. doi:10.1093/biostatistics/kxx069.

Xie, X., Wang, L., Yao, M., Wen, X., Chen, X., You, H., Jia, J., Zhao, J. and Lu, F. (2016) "Correlation between red blood cell count and liver function status." *Zhonghua Gan Zang Bing Za Zhi,* 24, 119-22. doi:10.3760/cma.j.issn.1007-3418.2016.02.009.

Yang, J., Yan, B., Yang, L., Li, H., Fan, Y., Zhu, F., Zheng, J. and Ma, X. (2018) "Macrocytic anemia is associated with the severity of liver impairment in patients with hepatitis B virus-related decompensated cirrhosis: a retrospective cross-sectional study." *BMC Gastroenterol,* 18, 161. doi:10.1186/s12876-018-0893-9.

Yoshiara, S., White, R. H., Raafat, F., Smith, N. C. and Shah, K. J. (1993) "Glomerular morphometry in reflux nephropathy: functional and radiological correlations." *Pediatr Nephrol,* 7, 15-22. doi:10.1007/BF00861553.

Zhang, Z., Wan, Z., Zhu, Y., Zhang, L., Zhang, L. and Wan, H. (2021) "Prevalence of malnutrition comparing NRS2002, MUST, and PG-SGA with the GLIM criteria in adults with cancer: A multi-center study." *Nutrition,* 83, 111072. doi:10.1016/j.nut.2020.111072.

Zhao, T.-Y., Cong, Q.-W., Liu, F., Yao, L.-Y. and Zhu, Y. (2021) "Nonlinear Relationship Between Macrocytic Anemia and Decompensated Hepatitis B Virus Associated Cirrhosis: A Population-Based Cross-Sectional Study." *Frontiers in Pharmacology,* 12. doi:10.3389/fphar.2021.755625.